ECS Journal of Solid State
Science and Technology



OPEN ACCESS

# Properties of Zirconium Oxide and Cobalt Ferrite Layered Nanocomposite

To cite this article: Aile Tamm *et al* 2017 *ECS J. Solid State Sci. Technol.* **6** P886

# Properties of Zirconium Oxide and Cobalt Ferrite Layered Nanocomposite

Aile Tamm,[a,z] Urmas Joost,[a] Mats Mikkor,[a] Kristjan Kalam,[a] Hugo Mändar,[a] Helina Seemen,[a] Joosep Link,[b] Raivo Stern,[b] Helena Castán,[c] Salvador Dueñas,[c] and Kaupo Kukli[a,d]

[a]Institute of Physics, University of Tartu, 50411 Tartu, Estonia
[b]National Institute of Chemical Physics and Biophysics, 12618 Tallinn, Estonia
[c]Department of Electronics, University of Valladolid, 47011 Valladolid, Spain
[d]Department of Chemistry, University of Helsinki, FI-00014 Helsinki, Finland

$CoFe_2O_4$ nanoparticles with 3–30 nm in diameter were synthesized by sol-gel method. The particles were spread as a solid discontinuous layer over planar silicon and TiN substrates by spin coating and covered by 15 nm thick $ZrO_2$ films by atomic layer deposition. Crystal structures distinctively characteristic of $CoFe_2O_4$ and $ZrO_2$ constituents were preserved. The nanocomposite $CoFe_2O_4$-$ZrO_2$ layers demonstrated dielectric polarization, saturative magnetization, and implications of resistive switching behavior. Behavior most clearly attributed to memory materials was observed in the field admittance characteristic with two distinct states in susceptibility of the nanocomposite.

 [DOI: 10.1149/2.0331712jss] 

Manuscript submitted October 25, 2017; revised manuscript received December 4, 2017. Published December 15, 2017.

There is permanent and growing interest in complex compound materials for a variety of applications in which the components tailor their best structural, mechanical, optical or electronic properties making the material versatile for the planned applications. Metal oxide based layered systems can demonstrate a variety of resistive switching, ferroelectric, ferromagnetic and other properties useful in prospective devices.[1] Cobalt-iron-oxygen ternary system has been of considerable interest, driven perhaps by the necessity of use it as a constituent compound in more complex structures exploited in solid oxide fuel cells.[2] Cobalt ferrite has been studied[3] as an attractive magnetic material suited to magneto-optical recording, integrated optics, or waveguides, due to its potential combination of semiconducting and magnetic properties including high coercivity, anisotropy, and magnetostriction.

$CoFe_2O_4$ particles have been earlier synthesized by mechanical milling and sintering of $Fe_2O_3$ and $Co_3O_4$ powders,[4] forced hydrolysis of ionic Co(II) and Fe(III) salts at 160°C in polyol medium,[5] thermal decomposition and/or direct micellar routes from cobalt(II) acetylacetonate and iron(III)acetylacetonate,[6,7] co-precipitation and/or micelles methods from iron and cobalt chlorides,[8,9] hydrothermally from chlorides[10,11] or nitrates,[12] solvothermal from Fe chloride and Co acetate,[13] solution combustion[14] and sol-gel from cobalt and iron nitrates,[15,16] or cobalt and iron acetylacetonates.[3]

Regarding other 3D structures based on cobalt ferrite, $Co_xFe_{3-x}O_4$ magnetic thin films have been grown on the pore walls of alumina membranes by atomic layer deposition.[17] Cobalt ferrite in thin film form has also been prepared by spray pyrolysis using cobalt and iron nitrate precursors.[18] Magnetization-field or Kerr loops with certain coercive force has earlier been recorded in $CoFe_2O_4$ particles[3–6,8,10,14,16] and thin films,[18] in most cases at room temperature. Ferromagnetic $CoFe_2O_4$ particles have been added to $YBa_2Cu_3O_{7-\delta}$ thin films to enhance flux pinning in potentially superconducting materials which, however, led to the formation of $Y(Fe,Co)O_3$, leaving the host material yttrium-deficient.[19] On the other hand, dilute Fe and Co co-doping into $ZrO_2$ has resulted in ferromagnetic behavior at room temperature for annealing temperatures above 900°C, suggesting that partial formation of secondary phases, such as cobalt ferrite, promoted ferromagnetism.[20] Very small $CoFe_2O_4$ particles with diameter 4–6 nm alone have also demonstrated magnetization decreasing toward higher temperatures and have thus been described as superparamagnetic.[6,9] Coercive field decreased substantially with increasing temperature, although saturative magnetization could be achieved at room temperature as well.[5]

$CoFe_2O_4$ particles embedded in $SiO_2/ZrO_2$ host matrix have been studied and characterized as magneto-optical isolators and described as promising candidates for this application theoretically, with proposition to deposit corresponding composites by sol-gel method.[21,22] $CoFe_2O_4$ nanoparticles forming a ferrofluid led through sol could therewith be prepared by co-precipitation of corresponding metal hydroxides.[23] The latter composite materials layers would be able to demonstrate considerable Faraday rotation with the degree increasing with the content of $CoFe_2O_4$ particles. Zirconium oxide was herewith used to adjust the refractive index of the structure to meet the fundamental waveguiding conditions.

It seems that nanocomposites consisting of $CoFe_2O_4$ particles and $ZrO_2$ thin films grown by atomic layer deposition (ALD) have not yet been prepared. On the other hand, $CoFe_2O_4$ - $TiO_2$ nanostructures have been elaborated using colloidal chemistry and ALD.[24] Electrospun $CoFe_2O_4$ microfibers have also conformally coated by ALD-grown $TiO_2$.[25] However, cobalt ferrite thin films have also been grown by ALD on porous monoclinic $ZrO_2$ supporting substrates.[26]

This study was devoted to the application of atomic layer deposition for coating the cobalt ferrite nanoparticles with thin zirconium dioxide films. The structure, electrical and magnetic performances of the resulting composites were addressed. Potential of the composite material to demonstrate both electrical and magnetic polarization was evaluated.

## Experimental

The particles were synthesized analogously to the method described by Ammar et al.[5] with slight modifications to the synthesis procedure. The synthesis procedure was following: 1.62 g (0.006 mol) of $FeCl_3 \cdot 6\,H_2O$, 0.747 g (0.003 mol) of $Co(CH_3COO)_2 \cdot 4\,H_2O$ and 2.214 g (0.027 mol) of $CH_3COONa$ were dissolved in 30.0 g propylene glycol. One gram of acetyl acetone was added, and the mixture was refluxed for five hours. After the completion of the reaction, the mixture was cooled and centrifuged. The particles were washed twice with acetone and dispersed in butanol.

X-ray photoelectron spectroscopy (XPS) was used for investigating the chemical state and elemental composition of cobalt iron oxide nanoparticle-based films after different treatments. XPS measurements were conducted using a surface station equipped with an electron energy analyzer (SCIENTA SES 100) and a non-monochromatic twin anode X-ray tube (Thermo XR3E2), with characteristic energy of 1253.6 eV (Mg $K_{\alpha 1,2}$ FWHM 0.68 eV). All XPS measurements were conducted in Ultra-High Vacuum (UHV) with a base-pressure better than $8 \times 10^{-10}$ mbar.

[z]E-mail: aile.tamm@ut.ee

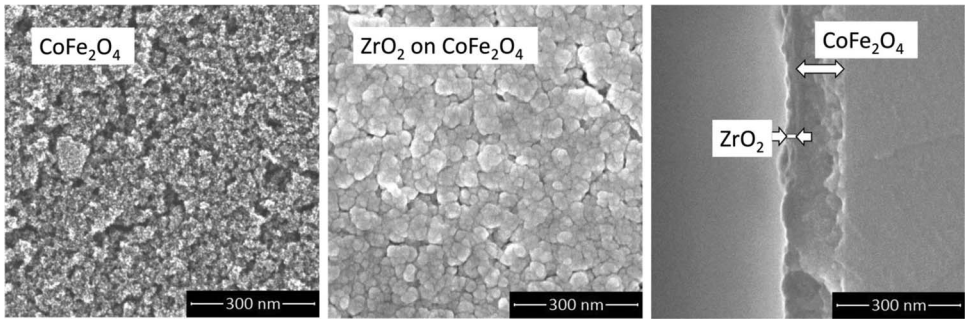


**Figure 1.** Bird-eye scanning electron microscopy images of $CoFe_2O_4$ particle layer (left panel), $CoFe_2O_4$ particles coated with $ZrO_2$ film (middle panel) and cross-sectional view on $CoFe_2O_4$ particles coated with $ZrO_2$ film (right panel).

Size of $CoFe_2O_4$ particles was characterized by small angle X-ray scattering (SAXS) analysis on diffractometer SmartLab (Rigaku) by using SAXS optics. Concentration of $CoFe_2O_4$ particles in butanol was 4.5 mass % for all three samples (nr. 2,3,4). Butanol was used as a buffer for background correction. Mark capillary tubes (0.7 mm diameter) were used for sample holders. Scattering data analysis was performed by program NanoSolver (Rigaku).

$ZrO_2$ films were grown in a low-pressure (200–260 Pa) flow-type in-house built hot-wall ALD reactor[27] at 300°C from zirconium tetrachloride, $ZrCl_4$ (Aldrich, 99.99%) and ozone, $O_3$. Nitrogen, $N_2$ (99.999% purity, AGA), was applied as the carrier and purging gas. $ZrCl_4$ was evaporated at 170°C from open boats inside the reactor. Ozone was produced from $O_2$ (99.999% purity, AGA) using BMT Messtechnik 802 N generator. The ozone concentration, measured by BMT Messtechnik 964 analyzer, was 245–250 g/m$^3$ in the experiments. The estimated ozone flow rate from the generator was about 67 sccm, while the carrier gas flow rate was kept at about 220 sccm. The ALD cycle times were 5 s for Zr precursor and ozone pulses as well as purge periods.

$ZrO_2$ films were grown on spin-coated $CoFe_2O_4$ particles as well as reference Si(100) substrates covered by chemically grown 1–2 nm thick $SiO_2$. In additon, highly-doped conductive Si substrates covered by 10 nm thick TiN film grown by chemical vapor deposition were used as bottom electrodes. For electrical measurements, the particles, covered with $ZrO_2$ film after spreading on TiN substrates, were supplied with platinum electrodes electron-beam evaporated on top of the films.

The crystal structure was evaluated by grazing incidence X-ray diffractometry (GIXRD), using an X-ray diffractometer SmartLab (Rigaku). X-ray fluorescence (XRF) spectrometer Rigaku ZSX 400 and program ZSX Version 5.55 was used to evaluate the elemental composition of films. Surface morphology of films and a cross-section of an ALD coated stack was evaluated by scanning electron microscopy (SEM) using a Dual Beam equipment (FEI Company) Helios NanoLab 600.

Electrical measurements were carried out by means of a semiconductor analyzer (Keithley 4200SCS), with samples put in a light-tight and electrically shielded box. The DC voltage was applied to the top electrode, being the bottom one grounded. To carry out the admittance parameters recording, a small signal of 30 mV r. m. s. was overlapped to the DC bias voltage. A parallel admittance model was selected which directly provides the real component value of the admittance (conductance, G) and the imaginary one (capacitance, C). The measurement frequency was varied between 1 kHz and 1 MHz. Additional electrical measurements were also carried out by means of an Agilent DXO-X 3104 digital oscilloscope with a built-in wave generator. Herewith the standard Sawyer-Tower experiment was carried out by applying a periodic triangular-shaped stimulus and recording the voltage loops data from the oscilloscope. Charge values were obtained from the sensed voltage across a stated capacitance.

Magnetometry was performed using Vibrating Sample Magnetometer (VSM) option of the Physical Property Measurement System 14T (Quantum Design) by scanning the magnetic field from −1 to 1 T parallel to the film surface at room temperature.

## Results and Discussion

The thickness of $ZrO_2$ thin films grown using 150 ALD cycles was 15 nm, allowing one to consider average growth rate for the zirconium oxide as high as 0.1 nm/cycle. The average thickness of layer consisting of $CoFe_2O_4$ particles spread on silicon substrate by spin-coating was 120 nm. Figure 1 presents SEM images of non-coated particles as well as $ZrO_2$ film deposited on particles.

Visual inspection of the nanocomposites revealed that the layer consisting of the ferrite particles only is, evidently, rather rough with features implying porous surface. ALD process of $ZrO_2$ films tended to conformally coat the particles without complete filling of the pores. However, the whole composite is not to be considered as porous throughout the whole 100–150 nm thickness, as the cross-section image has revealed appreciably uniform and continuous layer coating the silicon substrate (Fig. 1).

The small-angle X-ray scattering patterns of all samples were almost identical showing a fast decrease of intensity at low scattering angles ($2\theta < 0.6^\circ$) and a broad halo around scattering angles 0.7–2.0 (not shown). This shape of SAXS pattern did not allow approximations by using mono-modal size distribution function. Instead, a bimodal size distribution gave the best match to the observed scattering patterns with residual error R = 1.5%. The average diameters of particles corresponding to the first and second size distributions were 3.6(3) nm and 32(2) nm, respectively. Relative volume factions of both distributions were equal to 0.5(1) although the broadening of the first distribution was about two times smaller compared to the second distribution (Fig. 2).

It is not clear what exactly has caused the bimodal division of the ferrite particles between sets of two different average sizes. It might,

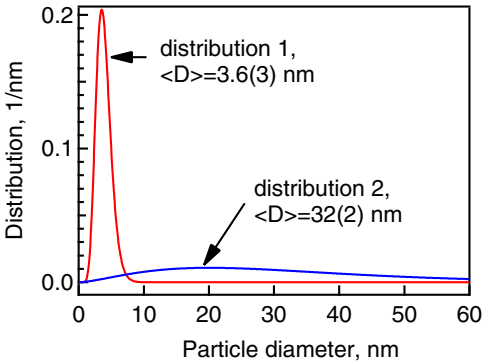


**Figure 2.** Particle size distributions of $CoFe_2O_4$ nanoparticles in butanol, calculated from SAXS analysis.

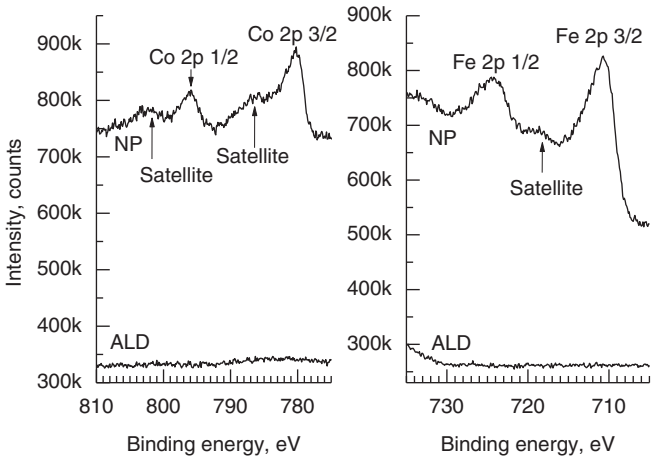


**Figure 3.** XPS spectra of cobalt ferrite nanoparticles denoted as NP, and nanoparticles covered by ALD $ZrO_2$ films, denoted as ALD.

however, be possible, that the smallest particles are those grown to the minimum sizes enabling short-range ordering and thus forming the nanocrystallites, whereas the larger particles may be formed because of the agglomeration of smaller ones neighboring each other.

In the XPS spectra of the $CoFe_2O_4$ nanoparticles, Co 2p, and Fe 2p lines were clearly visible (Fig. 3). Also, O 1s and residual C 1s lines were recorded at 530 and 280 eV, respectively, and some slight traces of residual chlorine could be observed at 285 eV (not shown).

In the Co 2p spectrum, Co 2p3/2 peak was identified at 780.7 eV and Co 2p1/2 at 796.1 eV, in addition, satellite peaks were identified at 786.2 and 802.3 eV respectively. Based on the location of the Co 2p photo lines and the satellite structures, cobalt was identified as $Co^{2+}$.[28,29] Fe 2p lines indicated that iron is in $Fe^{3+}$ oxidation state, while the existence of the satellite peak at 719.3 eV serves as clear evidence of $Fe^{3+}$ in the structures deposited.[30] On the ALD covered nanoparticle films, Zr 3d lines at 182.3 and 184.5 eV appeared (not shown), but Fe 2p and Co 2p lines were not visible any more (Fig. 2).

Figure 4 depicts X-ray diffraction patterns from reference $ZrO_2$ films, $CoFe_2O_4$ particles alone, and $ZrO_2/CoFe_2O_4$ composite layers.

The GIXRD patterns taken from reference $ZrO_2$ films (Fig. 4) revealed polycrystalline nature of the film consisting of metastable cubic (PDF Card 027-0997) or tetragonal (PDF Card 70-6628) and stable monoclinic (ICPDS Card 96-210-0389) polymorphs. The $CoFe_2O_4$ particles were evidently true nanocrystals decided after their XRD

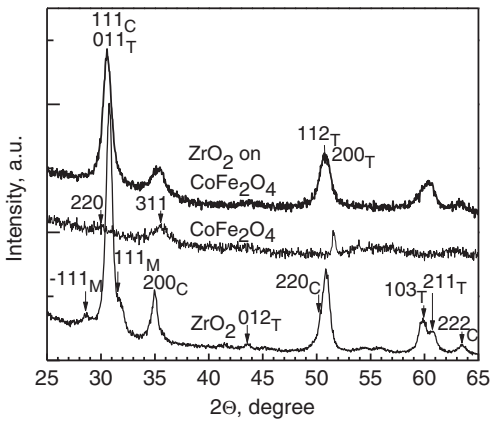


**Figure 4.** GIXRD patterns of three samples: 150 × $ZrO_2$ cycles on $CoFe_2O_4$ nanoparticles (top pattern), $CoFe_2O_4$ nanoparticles layered by spin-coating on Si (middle pattern), and $ZrO_2$ reference film grown using 250 ALD cycles (bottom pattern).

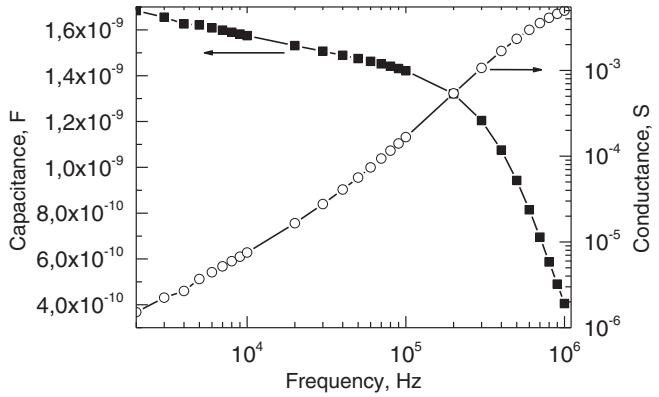


**Figure 5.** Capacitance and conductance dispersion curves, measured on 0.204 $mm^2$ dot electrodes. Pt/$ZrO_2$: $CoFe_2O_4$ /TiN/Si/Al structure. 150 cycles $ZrO_2$ were deposited on spin-coated $CoFe_2O_4$ particles.

patterns revealing only two low-intensity and broad peaks attributable to cubic $CoFe_2O_4$ phases (PDF Cards 003-0864 and 022-1086).

Figure 5 demonstrates frequency dependences of capacitance and conductance of the $ZrO_2/CoFe_2O_4$ composite layers formed between conductive TiN/Si and platinum electrodes. One can see that the films exhibited marked dispersion characteristic of electronically polarizable dielectric materials.

Relative permittivity values characterizing $ZrO_2$ films embedding $CoFe_2O_4$ particles were calculated on the basis on simple parallel plate capacitor model with $CoFe_2O_4$ particle layer with thickness of 115 nm covered by $ZrO_2$ layer grown to thickness of 15 nm, resulting in values of 110.4, 100.4, 89.7, and 25.3 at 1, 10, 100, and 1000 kHz, respectively.

For comparison to the literature data, Gutiérrez et al. have reported the dielectric permittivity of 14, i.e. the value close to that of the bulk phase, for epitaxial $CoFe_2O_4$ films.[31] However, in the same study considerable permittivity dispersion was revealed, indicating the permittivity values as high as 200 and above that at measurement frequency at 1 kHz. This was proposedly arising from nonintrinsic polarization processes, such as interfacial polarization due to internal leakage and consequent formation of large capacitance on Schottky barriers at the oxide-electrode interfaces.[31] At frequencies exceeding 100 kHz the permittivity was reduced below 25, which was regarded as a reasonable value. Analogously, very large values of dielectric permittivity reaching and exceeding several hundreds were measured for powders consisting of $CoFe_2O_4$ nanoparticles with sizes ranging from 6 to 30 nm.[32] The apparent permittivity values were found to increase markedly with the decrease in both particle size and measurement frequency, being indicative of the role for grain boundary conduction and accompanying interfacial polarization. Further, in another study on $CoFe_2O_4$ sintered at 400°C from sol-gel synthesized powders, initially consisting of particles with size 6–50 nm, the room-temperature permittivity was 18.6, measured at 1 kHz.[33] In the present study, one can, based on permittivity values obtained, thus also consider quite dense layer of ferrite particles formed with marked increment of effective permittivity at relatively low measurement frequencies due to considerable leakage currents in the composite.

Figure 6 depicts the electroforming process and the subsequent bipolar switching of the current.

The application of a voltage of around 6.4 V with a current compliance of 2 mA, to avoid the irreversible breakdown of the dielectric films, probably led to the formation of conductive filaments. Then, the conduction between top and bottom electrodes was enabled and the switching process activated. I-V cycles could excellently be repeated but with a rather narrow window remained between ON and OFF states, less than one order of magnitude. The low resistance state (ON state) was achieved by applying a negative voltage bias of −2 V (Fig. 6), whereas the high resistance state (OFF state) was reached when applying a positive voltage of +1.5 V.

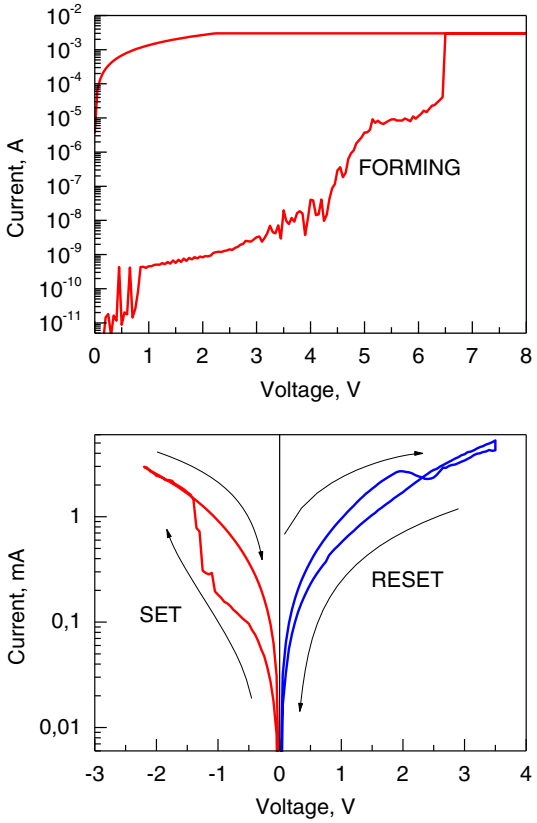


**Figure 6.** Current-voltage curves measured from Pt/$ZrO_2$: $CoFe_2O_4$ /TiN/Si/Al structure with $ZrO_2$ film deposited using 150 ALD cycles on spin-coated $CoFe_2O_4$ particles revealing the first forming cycle (upper panel) and bipolar resistive switching cycles (lower panel).

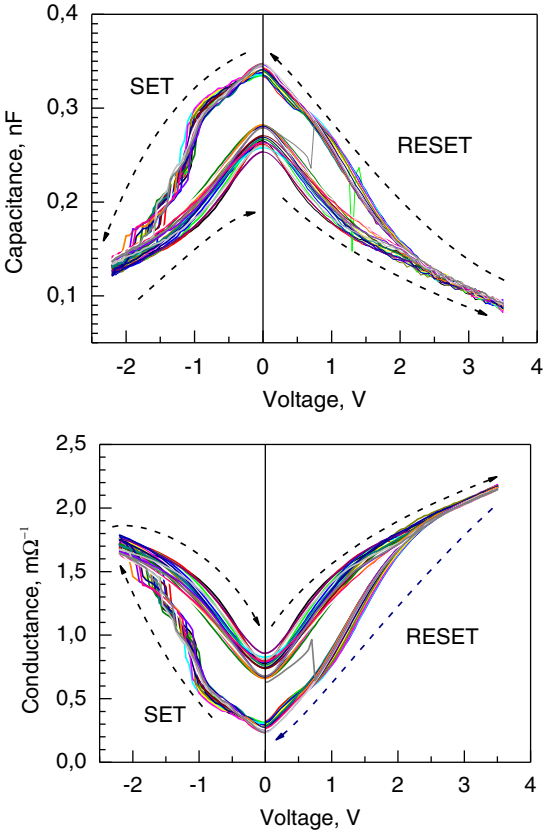


**Figure 7.** Capacitance-voltage (upper panel) and conductance-voltage (lower panel).

Studies on $CoFe_2O_4$ as resistive switching material have been relatively scarce compared to several other metal oxide films. Resistive switching behavior has been observed and described, e.g., in $CoFe_2O_4$ films electrodeposited on porous alumina templates[34] and chemical solution deposited on planar platinum electrodes.[35]

Figure 7 demonstrates capacitance-voltage and admittance (conductance) – voltage loops measured from the same composite sample. The measured magnitudes in there are conductance as the real part of the admittance, and capacitance as the imaginary part of the admittance.

Small signal parameters, both conductance and capacitance, also show switching loops with good repetitiveness, as it is shown in Fig. 7 for 20 consecutive cycles obtained at 100 kHz. As it has been recently demonstrated,[36] in samples exhibiting bipolar resistive switching, both the phase (conductance, G) and positive quadrature (capacitance, C) components of admittance show hysteretic behavior. Similarly, to set and reset current loops, G-V and C-V curves constitute two different lobes at positive and negative voltages, respectively. These loops were, in the present study, reproducible with an appreciable window for 20 consecutive cycles measured at 100 kHz. Figure 8 demonstrates capacitance and conductance loops as the components of admittance, measured separately against positive and negative sweeps of applied voltage. Both values were registered after returning to zero voltage after each programming voltage pulse.[37]

Memory cycles were obtained by using a return-to-zero pulse voltage sequence: 0 V (1 ms) → programming voltage V of 1 ms → 0 V (1 ms), with the programming voltage V following a double ramp ranging from +3.5 V to −2 V with −0.1 V steps. Admittance signal was recorded at reading voltage of 0 V to discard any disturbance of the measurement process to possible conductive filaments responsible of the conduction. Figure 7 depicts the conductance and capacitance

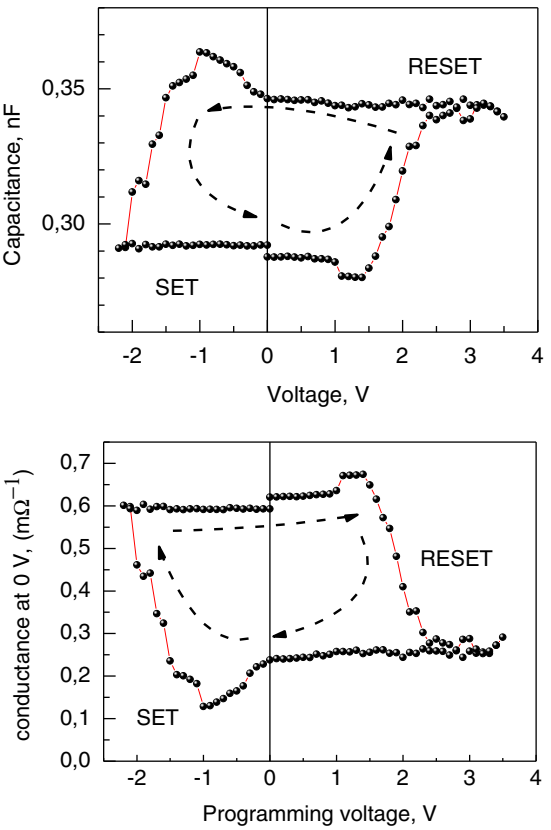


**Figure 8.** Capacitance (upper panel) and conductance (lower panel) behavior against programming peak voltage, registered at 0 V.

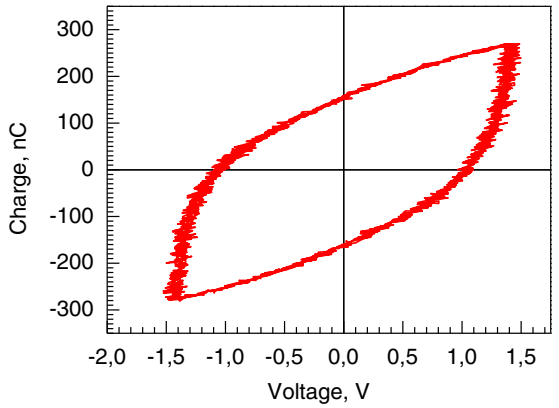


**Figure 9.** Charge on sense capacitor versus voltage applied on $Pt/ZrO_2$:$CoFe_2O_4$ /TiN/Si/Al structure as a sample capacitor in series with 100 nF sense capacitor in Sawyer-Tower circuit. 150 cycles $ZrO_2$ were deposited on spin-coated $CoFe_2O_4$ particles.

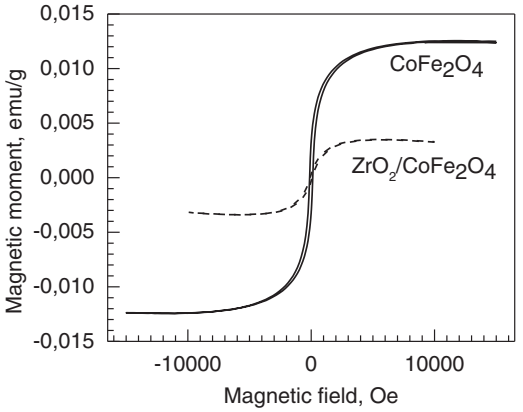


**Figure 10.** Magnetization versus field loops for $CoFe_2O_4$ nanopowder and $CoFe_2O_4$ nanoparticle layer covered by 15 nm thick $ZrO_2$ film, designated by labels.

values, respectively, measured at 0 V as functions of the programming voltage. The ON and OFF states are clearly distinguished. One can thus see, that two different states of memory can be sensed and fixed at 0 V after each programming cycle.

Figure 9 depicts an electrical charge versus voltage loop measured using Sawyer-Tower circuit.

One can see in Fig. 9, that, despite the obvious hysteresis in the charge-voltage loop, saturation regime for the electrical polarization is not quite achieved at either polarity of the external field, as the polarized charge kept increasing with the voltage. This kind of charge behavior is hardly to be regarded as that characteristic of defined ferroelectric material, although very weak implications of certain tendency to saturative charge polarization might be recognized at the highest voltages used. The currents through the materials layer, as measured, have indeed been considerably high (Fig. 5). Most probably, most of the charge, responsible for the effectively measurable polarization in the material deposited, was that drifting in the electric field from an electrode to the counter electrode. That charge, either electronic or ionic, could become trapped at the interfaces between metal oxide layer and the electrode evaporated, giving rise to the interfacial polarization. Consequently, the electrical charge becomes carried to and trapped at the interface layer under certain polarity, and an opposite polarity with increasing, oppositely directed, field is required to release the charge from the traps and for the following drift toward the counter electrode. On the other hand, somewhat analogous polarization-field behavior has been observed and recorded in Ti-doped $CoFe_2O_4$ ceramics[38] or in nanostructures containing thin layers $Fe_2O_3$ and $Co_3O_4$,[39] or $Er_2O_3$ and $Fe_2O_3$,[40] and still considered promising in terms of multiferroic performance of the material.

The ferrite nanoparticles as well as the layer of nanoparticles covered by $ZrO_2$ film demonstrated saturate behavior in magnetization-field curves, together with narrow hysteresis otherwise characteristic of soft ferromagnetic materials (Fig. 10).

$CoFe_2O_4$ is a well-known magnetic material also possessing noticeable magnetocrystalline anisotropy within its cubic lattice.[41] In our study, the coercive fields, $H_C$, for $CoFe_2O_4$ nanopowder and $CoFe_2O_4$ nanoparticle layer covered by $ZrO_2$ film were 130 and 70 Oe, respectively (Fig. 10). For comparison with literature data, saturation magnetization, remnant magnetization, and coercive field measured from powders of $CoFe_2O_4$ nanoparticles with average size of 34 nm, synthesized by hydrothermal method have been 56.88 emu/g, 21.44 emu/g, and 507.8 Oe, respectively.[42] In another study, the corresponding values measured from hydrothermally synthesized and annealed powders consisting of particles with average size of 20 ± 2 nm reached 59–60 emu/g, 23 emu/g, and 570–650 Oe, respectively.[12] Yet in another study on hydrothermally synthesized $CoFe_2O_4$ particles of 12–22 nm in diameter, the coercive field was as high as 1.69 kOe, together with the saturation and remanent magnetizations of 82 emu/g and 33 emu/g, respectively.[43] Furthermore, single crystal $CoFe_2O_4$ sub-microspheres obtained by solvothermal method have shown ferromagnetic behavior with saturation magnetization ($M_{sat}$) value of 63.1 emu/g and coercivity ($H_c$) value of 574.1 Oe, whereas particles with size less than 9 nm went superparamagnetic at room temperature showing no hysteresis.[13] Magnetometry of $CoFe_2O_4$ particles with size of 5 nm synthesized by hydrothermal method[12] has revealed maximum saturation magnetization and coercivity of 68.9 emu/g and 340.6 Oe, respectively. In $CoFe_2O_4$ particles by thermal plasma assisted gas condensation method[44] saturation magnetization was 61–70 emu/g and the coercivity 552–849 Oe.

Figure 11 depicts magnetization-field curves measured from the nanocomposite $CoFe_2O_4$-$ZrO_2$ layer at room temperature (300 K) and at as low temperature as 5 K.

The saturation magnetization, $M_{sat}$, in ferromagnetic polarization regime at $5.12 \times 10^{-5}$ emu. Coercivity value, $H_C$, reached 17.3(5) kOe. Remanent magnetization, $M_r$, was estimated as high as $4.293 \times 10^{-5}$ emu. Thus, the squareness of the ***M-H*** loop, $M_r/M_{sat}$, was as high as 0.838. For comparison, in pellets consisting of $Co_{1.5}Fe_{1.5}O_4$ nanoparticles with the size ranging from 9 to 40 nm fabricated in co-precipitation process from $Co(NO_3)_2 \cdot 6H_2O$ and $Fe(NO_3)_3 \cdot 9H_2O$ salts, coercivity and squareness values of 11–16 kOe and 0.70–0.92, quite comparable to those obtained in the present study, were measured at 4 K.[45] The maximum values were obtained in the case of average nanograin size of approximately 16 nm. Differently from the

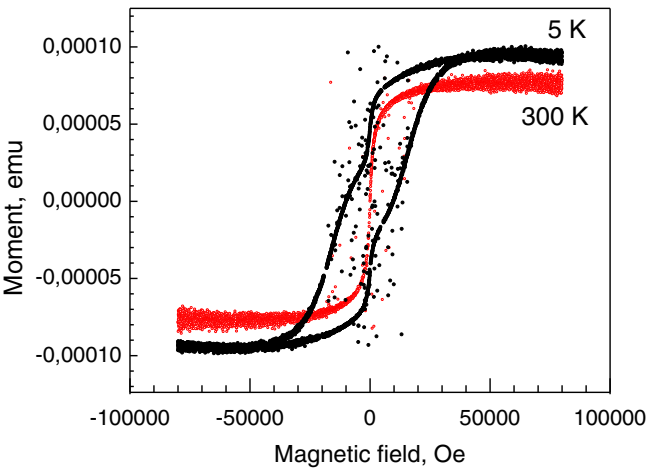


**Figure 11.** Magnetization-field curves from $CoFe_2O_4$ nanoparticle layer covered by 15 nm thick $ZrO_2$ film, measured at 5 and 300 K.

present study, in the pellet samples certain coercivity and squareness, 35–320 Oe and 0.007-0.333, repectively, were obtained also at room temperature.

It is to be considered, that both $CoFe_2O_4$ and $ZrO_2$ layers may be magnetized separately. Also $ZrO_2$, especially when stabilized dominantly in its metastable tetragonal polymorph, can demonstrate saturative magnetization and hysteresis in magnetization-field curves.[46] In our sample, humps apparent in the ***M-H*** loop during the increasing and decreasing magnetization (Fig. 10) may be indicative of the exchange coupling between magnetizing layers, i.e. bias effect due to the interaction between base $CoFe_2O_4$ particle layer and the $ZrO_2$ film deposited on top of it, resulting in the re-orientation of the polarization in base and vicinal layers at different times during the overall polarization process under the increasing external field.

## Summary

$CoFe_2O_4$ nanoparticles with bimodal size distribution (mean sizes 3.6 and 32 nm), synthesized by sol-gel method, were spread by spin-coating as uniform ca. 100 nm thick layer of particles on silicon substrates. The layer of particles was homogeneously coated by 15 nm thick, dominantly tetragonal/cubic, $ZrO_2$ film grown by atomic layer deposition. The nanocomposite layered structures formed were characterized in terms of their capacitive properties, current switching and magnetoelectric behavior. The capacitor-like samples demonstrated marked dielectric dispersion with relative permittivity 25 of the double $CoFe_2O_4$-$ZrO_2$ layer at 100 kHz and above that measurement frequency. Significant role for leakage currents through the material could be considered. The composite layer also demonstrated clear tendency to resistive switching behavior via alternate formation of states of two different current density values. Measurements in resistive switching regime became feasible after application of a forming voltage of around 6.4 V. Loops between extremal charge values of 300 nC, approximately, on capacitors of 0.204 $mm^2$ area were recorded also in the electrical polarization charge – voltage/field behavior, presumably also affected by the interfacial polarization during voltage sweeps. In addition, the composite layers could also be saturatively magnetized in external magnetic fields, demonstrating magnetization-field hysteresis loops with low coercivity characteristic of soft ferromagnetic like materials. At low temperatures, the coercivity exceeded 17 kOe. The squareness of the ***M*** - ***H*** loop was higher than 0.8. The clearest behavior attributable to that of potential memory materials was, however, achieved and demonstrated in the capacitance-conductance measurement regime, allowing one to achieve well-defined, highly quadratic, loops in admittance-programming voltage behavior, revealing two distinct functional states in the susceptibility of the external electric field.

## Acknowledgments

This work was partially funded by the European Regional Development Fund project "Emerging orders in quantum and nanomaterials" (TK134), Estonian Research Council Grants IUT2-24 and PUTJD680, Estonian Academy of Sciences (SLTFYPROF) and Spanish Ministry of Economy and Competitiveness (TEC2014-52152-C3-3-R) with support of Feder funds.

## ORCID

Aile Tamm https://orcid.org/0000-0002-0547-0824
Raivo Stern https://orcid.org/0000-0002-6724-9834

## References

1. K. Kalantar-zadeh, J. Z. Ou, T. Daeneke, A. Mitchell, T. Sasaki, and M. S. Fuhrer, "Two dimensional and layered transition metal oxides," *Appl. Mater. Today*, **5**, 73 (2016).
2. W.-W. Zhang and M. Chen, "Thermodynamic modeling of the Co–Fe–O system," *CALPHAD: Computer Coupling of Phase Diagrams and Thermochemistry*, **41**, 76 (2013).
3. D. Erdem, N. S. Bingham, F. J. Heiligtag, N. Pilet, P. Warnicke, L. J. Heyderman, and M. Niederberger, "$CoFe_2O_4$ and $CoFe_2O_4$-$SiO_2$ nanoparticle thin films with perpendicular magnetic anisotropy for magnetic and magneto-optical applications," *Adv. Funct. Mater.*, **26**, 1954 (2016).
4. S. B. Waje, M. Hashim, W. D. W. Yusoff, and Z. Abbas, "X-ray diffraction studies on crystallite size evolution of $CoFe_2O_4$ nanoparticles prepared using mechanical alloying and sintering," *Appl. Surf. Sci.*, **256**, 3122 (2010).
5. S. Ammar, A. Helfen, N. Jouini, F. Fiévet, I. Rosenman, F. Villain, P. Moliniéd, and M. Danot, "Magnetic properties of ultrafine cobalt ferrite particles synthesized by hydrolysis in a polyol medium," *J. Mater. Chem.*, **11**, 186 (2001).
6. D. Peddis, C. Cannas, A. Musinu, A. Ardu, F. Orrù, D. Fiorani, S. Laureti, D. Rinaldi, G. Muscas, G. Concas, and G. Piccaluga, "Beyond the effect of particle size: Influence of $CoFe_2O_4$ nanoparticle arrangements on magnetic properties," *Chem. Mater.*, **25**, 2005 (2013).
7. L. T. Lu, N. T. Dung, L. D. Tung, C. T. Thanh, O. K. Quy, N. V. Chuc, S. Maenosono, and N. T. K. Thanh, "Synthesis of magnetic cobalt ferrite nanoparticles with controlled morphology, monodispersity composition: the influence of solvent, surfactant, reductant and synthetic conditions," *Nanoscale*, **7**, 19596 (2015).
8. I. Sharifi, H. Shokrollahi, M. M. Doroodmand, and R. Safi, "Magnetic and structural studies on $CoFe_2O_4$ nanoparticles synthesized by co-precipitation, normal micelles and reverse micelles methods," *J. Magn. Magn. Mater.*, **324**, 1854 (2012).
9. C. Pereira, A. M. Pereira, C. Fernandes, M. Rocha, R. Mendes, M. P. Fernández-García, A. Guedes, P. B. Tavares, J.-M. Grenèche, J. P. Araújo, and C. Freire, "Superparamagnetic $MFe_2O_4$ (M = Fe, Co, Mn) nanoparticles: Tuning the particle size and magnetic properties through a novel one-step coprecipitation route," *Chem. Mater.*, **24**, 1496 (2012).
10. S. C. Goh, C. H. Chia, S. Zakaria, M. Yusoff, C. Y. Haw, Sh. Ahmadi, N. M. Huang, and H. N. Lim, "Hydrothermal preparation of high saturation magnetization and coercivity cobalt ferrite nanocrystals without subsequent calcination," *Mater. Chem. Phys.*, **120**, 31 (2010).
11. I. Zalite, G. Heidemane, L. Kuznetsova, and M. Maiorov, "Hydrothermal synthesis of cobalt ferrite nanosized powders," *IOP Conf. Series: Mater. Sci. Eng.*, **77**, 012011 (2015).
12. D. Zhao, X. Wu, H. Guan, and E. Han, "Study on supercritical hydrothermal synthesis of $CoFe_2O_4$ nanoparticles," *J. Supercrit. Fluids*, **42**, 226 (2007).
13. L. Cui, P. Guo, G. Zhang, Q. Li, R. Wang, M. Zhou, L. Ran, and X. S. Zhao, "Facile synthesis of cobalt ferrite submicrospheres with tunable magnetic and electrocatalytic properties," *Coll. Surf. A: Physicochem. Eng. Asp.*, **423**, 170 (2013).
14. V. Kaliyamoorthy, D. R. Babu, and M. Saminathan, "Impact of ignition temperature on particle size and magnetic properties of $CoFe_2O_4$ nanoparticles prepared by self-propagated MILD combustion technique," *J. Magn. Magn. Mater.*, **418**, 280 (2016).
15. B. Pacakova, A. Mantlikova, D. Niznansky, S. Kubickova, and J. Vejpravova, "Understanding particle size and distance driven competition of interparticle interactions and effective single-particle anisotropy," *J. Phys.: Condens. Matter*, **28**, 206004 (2016).
16. K. Kombaiah, J. J. Vijaya, L. J. Kennedy, M. Bououdina, R. J. Ramalingam, and H. A. Al-Lohedan, "Comparative investigation on the structural, morphological, optical, and magnetic properties of $CoFe_2O_4$ nanoparticles," *Ceram. Int.*, **43**, 7682 (2017).
17. G. Armelles, A. Cebollada, and A. García-Martín, "Magneto-optical properties of core−shell magneto-plasmonic Au−$Co_xFe_{3-x}O_4$ nanowires," *Langmuir*, **28**, 9127 (2012).
18. A. A. Bagade, V. V. Ganbavle, S. V. Mohite, T. D. Dongale, B. B. Sinha, and K. Y. Rajpure, "Assessment of structural, morphological, magnetic and gas sensing properties of $CoFe_2O_4$ thin films," *J. Coll. Interface Sci.*, **497**, 181 (2017).
19. S. C. Wimbush, R. Yu, R. Bali, J. H. Durrell, and J. L. MacManus-Driscoll, "Addition of ferromagnetic $CoFe_2O_4$ to YBCO thin films for enhanced flux pinning," *Physica C*, **470**, S223 (2010).
20. J. Okabayashi, S. Kono, Y. Yamada, and K. Nomura, "Fabrication and magnetic properties of Fe and Co co-doped $ZrO_2$," *AIP Adv.*, **1**, 042138 (2011).
21. M. Zamani and A. Hocini, "Large Faraday rotation in magnetophotonic crystals containing $SiO_2$/$ZrO_2$ matrix doped with $CoFe_2O_4$ magnetic nanoparticles," *Opt. Mater.*, **58**, 306 (2016).
22. M. Zamani and A. Hocini, "Potential of $SiO_2$/$ZrO_2$ matrix doped with $CoFe_2O_4$ magnetic nanoparticles in achieving integrated magneto-optical isolators," *Photonics and Nanostructures – Fundamentals and Applications*, **24**, 41 (2017).
23. F. Choueikani, F. Royer, D. Jamon, A. Siblini, J. J. Rousseau, S. Neveu, and J. Charara, "Magneto-optical waveguides made of cobalt ferrite nanoparticles embedded in silica/zirconia organic-inorganic matrix," *Appl. Phys. Lett.*, **94**, 051113 (2009).
24. G. Clavel, C. Marichy, M.-G. Willinger, S. Ravaine, D. Zitoun, and N. Pinna, "$CoFe_2O_4$-$TiO_2$ and $CoFe_2O_4$-ZnO thin film nanostructures elaborated from colloidal chemistry and atomic layer deposition," *Langmuir*, **26**, 18400 (2010).
25. E. Santala, M. Kemell, M. Leskelä, and M. Ritala, "The preparation of reusable magnetic and photocatalytic composite nanofibers by electrospinning and atomic layer deposition," *Nanotechnology*, **20**, 035602 (2009).
26. J. R. Scheffe, Mark, D. Allendorf, E. N. Coker, B. W. Jacobs, A. H. McDaniel, and A. W. Weimer, "Hydrogen production via chemical looping redox cycles using atomic layer deposition synthesized iron oxide and cobalt ferrites," *Chem. Mater.*, **23**, 2030 (2011).
27. T. Arroval, L. Aarik, R. Rammula, V. Kruusla, and J. Aarik, "Effect of substrate-enhanced and inhibited growth on atomic layer deposition and properties of aluminum–titanium oxide films," *Thin Solid Films*, **600**, 119 (2016).
28. K. Zhang, W. Zuo, Z. Wang, J. Liu, T. Li, B. Wang, and Z. Yang, "A simple route to $CoFe_2O_4$ nanoparticles with shape and size control and their tunable peroxidase-like activity," *RSC Adv.*, **5**, 10632 (2015).

29. N. V. Long, Y. Yang, T. Teranishi, C. M. Thi, Y. Cao, and M. Nogami, "Related magnetic properties of $CoFe_2O_4$ cobalt ferrite particles synthesised by the polyol method with $NaBH_4$ and heat treatment: new micro and nanoscale structures," *RSC Adv.*, **5**, 56560 (2015).
30. A. P. Grosvenor, B. A. Kobe, M. C. Biesinger, and N. S. McIntyre, "Investigation of multiplet splitting of Fe 2p XPS spectra and bonding in iron compounds," *Surf. Interface Anal.*, **36**, 1564 (2004).
31. D. Gutiérrez, M. Foerster, I. Fina, J. Fontcuberta, D. Fritsch, and C. Ederer, "Dielectric response of epitaxially strained $CoFe_2O_4$ spinel thin films," *Phys. Rev. B*, **86**, 125309, (2012).
32. D. Rathore, R. Kurchania, and R. K. Pandey, "Influence of particle size and temperature on the dielectric properties of $CoFe_2O_4$ nanoparticles," *Int. J. Min. Metall. Mater.*, **21**, 408 (2014).
33. A. Arunkumar, D. Vanidha, K. Oudayakumar, S. Rajagopan, and R. Kannan, "Metallic magnetism and change of conductivity in the nano to bulk transition of cobalt ferrite," *J. Appl Phys.*, **114**, 183905 (2013).
34. C. Jiang, Lei Wu, W. W. Wei, C. Dong, and J. Yao, "The resistive switching memory of $CoFe_2O_4$ thin film using nanoporous alumina template," *Nanoscale Res. Lett.*, **9**, 584 (2014).
35. W. Hu, L. Zou, R. Chen, W. Xie, X. Chen, N. Qin, S. Li, G. Yang, and D. Bao, "Resistive switching properties and physical mechanism of cobalt ferrite thin films," *Appl. Phys. Lett.*, **104**, 143502 (2014).
36. S. Dueñas, H. Castán, H. García, E. Miranda, M. B. Gonzalez, and F. Campabadal, "Study of the admittance hysteresis cycles in TiN/Ti/$HfO_2$/W-based RRAM devices," *Microel. Eng.*, **178**, 30 (2017).
37. S. Dueñas, H. Castán, H. García, O. G. Ossorio, L. A. Domínguez, and E. Miranda, "Experimental observation of negative susceptance in $HfO_2$-based RRAM devices," *IEEE Electron Dev. Lett.*, **38**, 1216 (2017).
38. G. D. Dwivedi, Amish, G. Joshi, H. Kevin, P. Shahi, A. Kumar, A. K. Ghosh, H. D. Yang, and S Chatterjee, "Existence of the multiferroic property at room temperature in Ti doped $CoFe_2O_4$," *Solid State Comm.*, **152**, 360 (2012).
39. K. Kalam, H. Seemen, P. Ritslaid, M. Rähn, A. Tamm, K. Kukli, A. Kasikov, J. Link, R. Stern, S. Dueñas, H. Castán, and H. García, "Atomic layer deposition and properties of $ZrO_2$-$Fe_2O_3$ thin films," *Beilstein Journal of Nanotechnology*, accepted manuscript.
40. A. Tamm, K. Kalam, H. Seemen, J. Kozlova, K. Kukli, J. Aarik, J. Link, R. Stern, S. Dueñas, and H. Castán, "Magnetic and electrical performance of atomic layer deposited erbium-iron-oxide thin films," *ACS Omega*, **2**, 8836 (2017).
41. H. Shenker, "Magnetic anisotropy of cobalt ferrite ($Co_{1.01}Fe_{2.00}O_{3.62}$) and nickel cobalt ferrite ($Ni_{0.72}Fe_{0.20}Co_{0.08}Fe_2O_4$)," *Phys. Rev.*, **107**, 1246 (1957).
42. G. Allaedini, S. M. Tasirin, and P. Aminayi, "Magnetic properties of cobalt ferrite synthesized by hydrothermal method," *Int. Nano Lett.*, **4**, 183 (2015).
43. G. C. P. Leite, E. F. Chagas, R. Pereira, R. J. Prado, A. J. Terezo, M. Alzamora, and E. Baggio-Saitovitch, "Exchange coupling behavior in bimagnetic $CoFe_2O_4$/$CoFe_2$ nanocomposite," *J. Magn. Magn. Mater.*, **324**, 2711 (2012).
44. A. B. Nawale, N. S. Kanhe, K. R. Patil, V. R. Reddy, A. Gupta, B. B. Kale, S. V. Bhoraskar, V. L. Mathe, and A. K. Das, "Magnetic properties of nanocrystalline $CoFe_2O_4$ synthesized by thermal plasma in large scale," *Mater. Chem. Phys.*, **137**, 586 (2012).
45. R. N. Bhowmik, A. T. Satya, and A. Bharathi, "Synthesis of $Co_{1.5}Fe_{1.5}O_4$ spinel ferrite with high magnetic squareness and study its magnetic property by annealing the chemical routed sample at different temperatures," *J. Alloys Compd.*, **559**, 134 (2013).
46. S. Ning, P. Zhan, Q. Xie, Z. Li, and Z. Zhang, "Room-temperature ferromagnetism in un-doped $ZrO_2$ thin films," *J. Phys. D: Appl. Phys.*, **46**, 445004 (2013).